

Analysis of Axisymmetric Problems by Element-Free Galerkin Method

Ali Nemati Hayati, Mohammad Mehdi Ahmadi, and Seyed Amirodin Sadrnejad

Abstract—In this paper, mesh-free Element-Free Galerkin method has been utilized for analysis of axisymmetric problems. To this aim, basic formulations and assumptions of the method for the case of axisymmetry are derived, and a simple problem of linearly elastic solid mechanics is taken as a benchmark for controlling the consistency of the proposed formulation as well as its accuracy in comparison to FEM. Two different norms for error estimation, i.e. displacement & stress norm, have been addressed in this study. Eventually, using these two norms, a parametric study has been performed on critical factors to demonstrate suitable parametric values. The numerical results show high dependency of the predicted values to the selection of these parameters.

Index Terms—Axisymmetry, element-free galerkin method, error estimation, mesh-free

I. INTRODUCTION

Since the development of Element-Free Galerkin (EFG) method by T. Belytschko et al. [1], rather similarity of the method to the traditional FEM together with its higher accuracy, has made it the most well-known mesh-free method amid others. In the past, many aspects of this method have been addressed; and it has been used in solving many different problems of solid mechanics; such as crack propagation [2], [3], elasto plasticity [4], [5], large deformation [6] and lately in geomechanics [7], [8]. Three-dimensional problems have also been generally featured in the literature [2], [4]. While many problems of 3D nature have been analyzed by EFG method in two dimensions, application of the method to axisymmetry problems seems to have been inadequately addressed in the literature.

In this paper, the EFG formulation for the axisymmetry case is presented. The accuracy of the proposed method is verified by comparing the numerical results with analytical solution available for a known problem of linearly elastic solid mechanics.

To avoid confusion, in the following, the vectors and matrices are indicated by bold letters.

II. ELEMENT-FREE GALERKIN METHOD (EFGM)

There is one common feature in all mesh-free methods which differentiates them from element-based methods. This dividing border is the construction of shape functions just by a set of nodes without any contribution from elements in mesh-free methods. However, this condition does not interdict the use of elements for means of integration [9].

The Element-Free Galerkin (EFG) method can be described by its three main features. These are a) Moving Least Squares (MLS) approximation for creating shape functions, b) Galerkin weak form for deriving discretized system equations and c) a set of elements solely for integrating the system matrices, called background or integration mesh.

These features are explained in the following sections.

A. MLS Approximants

Let us assume that $u(x)$ is defined over domain Ω . The Moving Least Squares (MLS) approximation of $u(x)$ is indicated by $u^h(x)$ and is defined by:

$$u^h(\mathbf{x}) = \sum_j^m p_j(x) a_j(x) = \mathbf{P}^T(\mathbf{x}) \mathbf{a}(\mathbf{x}) \quad (1)$$

where $p_1(\mathbf{x})=1$ and $p_j(\mathbf{x})$ are monomials in the space coordinates $\mathbf{x}^T = [x, y]$, so as to make a complete basis. In this paper, linear polynomial basis is used.

$\mathbf{a}(\mathbf{x})$ should be determined in a way that sum of the weighted square residuals of nodal values and approximate values at nodes in a local domain, J , reaches a minimum value.

$$J = \sum_I^n w(\mathbf{x} - \mathbf{x}_I) [u^h(\mathbf{x}) - u_I]^2 \quad (2)$$

where $w(\mathbf{x} - \mathbf{x}_I)$ is a weight function and n is the number of nodes in a local domain called support domain of \mathbf{x} , in which $w(\mathbf{x} - \mathbf{x}_I) \neq 0$.

Finding the stationary of J in (2) with respect to $\mathbf{a}(\mathbf{x})$ leads to the following linear relation between $\mathbf{a}(\mathbf{x})$ and u_I :

$$\frac{\partial J}{\partial \mathbf{a}} = 0 \Rightarrow \mathbf{A}(\mathbf{x}) \mathbf{a}(\mathbf{x}) = \mathbf{B}(\mathbf{x}) \mathbf{U}_s \quad (3)$$

or

$$\mathbf{a}(\mathbf{x}) = \mathbf{A}^{-1}(\mathbf{x}) \mathbf{B}(\mathbf{x}) \mathbf{U}_s \quad (4)$$

where \mathbf{U}_s is the vector assembly of the nodal values in the support domain:

$$\mathbf{U}_s = [u_1, u_2, \dots, u_n]^T \quad (5)$$

Manuscript received July 19, 2012; revised August 25, 2012.

Ali Nemati Hayati is with the Department of Civil Engineering, Sharif University of Technology, Tehran, Iran (e-mail: alinhayati@mehr.sharif.ir).

Mohammad Mehdi Ahmadi is with the Department of Civil Engineering, Sharif University of Technology, Tehran, Iran (e-mail: mmahmadi@sharif.ir).

Seyed Amirodin Sadrnejad is with the Department of Civil Engineering, Khaje Nasir University of Technology, Tehran, Iran (e-mail: sadrnejad@hotmail.com).

$A(\mathbf{x})$ is the weighted moment matrix and is defined by:

$$A = \sum_{I=1}^n w(\mathbf{x} - \mathbf{x}_I) \mathbf{P}(\mathbf{x}_I) \mathbf{P}^T(\mathbf{x}_I) \quad (6)$$

and $B(\mathbf{x})$ is a matrix defined by the following Equation:

$$B_I = w(\mathbf{x} - \mathbf{x}_I) \mathbf{P}(\mathbf{x}_I) \quad (7)$$

By substituting (4) in (1), we have:

$$u^h(\mathbf{x}) = \sum_{I=1}^n \phi_I(\mathbf{x}) u_I \quad (8)$$

where $\phi_I(\mathbf{x})$ is the shape function which is governed by the following Equation:

$$\phi_I(\mathbf{x}) = \sum_{j=1}^m p_j(\mathbf{x}) (\mathbf{A}^{-1}(\mathbf{x}) \mathbf{B}(\mathbf{x}))_{ji} = \mathbf{P}^T \mathbf{A}^{-1} \mathbf{B}_I \quad (9)$$

Equation (8) can be written in the form:

$$u^h(\mathbf{x}) = \Phi(\mathbf{x}) \mathbf{U}_s \quad (10)$$

where

$$\Phi(\mathbf{x}) = [\phi_1(\mathbf{x}), \phi_2(\mathbf{x}), \dots, \phi_n(\mathbf{x})] \quad (11)$$

In this study, the following common and effective weight function is used [9]:

$$w(\mathbf{x} - \mathbf{x}_I) \equiv w(\bar{d}) = \begin{cases} \frac{2}{3} - 4\bar{d}^2 + 4\bar{d}^3 & \bar{d} \leq \frac{1}{2} \\ \frac{4}{3} - 4\bar{d} + 4\bar{d}^2 - \frac{4}{3}\bar{d}^3 & \frac{1}{2} < \bar{d} \leq 1 \end{cases} \quad (12)$$

where

$$\bar{d} = |\mathbf{x} - \mathbf{x}_I| / d_w = d / d_w \quad (13)$$

in which d_w is the size of the influence domain at a node and is computed by:

$$d_w = D_{\max} \times c_1 \quad (14)$$

where c_1 is the average nodal distance and D_{\max} is a scaling parameter called influence factor.

In this paper, advantage has been taken of rectangular influence domains for the nodes and identical influence factors for both directions.

Fig. 1 shows a rectangular influence domain of different size in two directions.

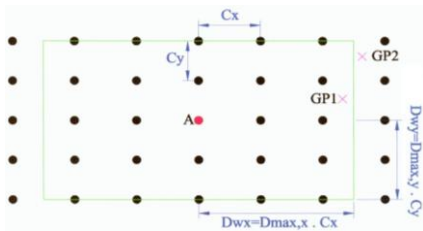


Fig. 1. Rectangular influence domain of a sample node A; Gauss points located inside this area are included for shape function creation and integration (e.g. GP1)

B. Deriving Discretized Variational Formulation in Axisymmetry

A general linearly elastic solid mechanics problem is used

to present the procedure of the EFG method in formulating the discretized system equations. The partial differential equation and boundary conditions for such a problem can be written in the form:

$$\mathbf{L}^T \boldsymbol{\sigma} + \mathbf{b} = 0 \quad \text{in problem domain } \Omega \quad (15)$$

$$\mathbf{u} = \bar{\mathbf{u}} \quad \text{on boundary } \Gamma_u \quad (16)$$

Equation (16) gives constraints to the field variable of displacements. The natural boundary conditions (traction forces) are given by:

$$\boldsymbol{\sigma} \mathbf{n} = \bar{\mathbf{t}} \quad \text{on natural boundary } \Gamma_s \quad (17)$$

In these equations, L is the differential operator, $\boldsymbol{\sigma}$ is the stress vector, b is the body force vector, u is the displacement vector, $\bar{\mathbf{t}}$ is the traction force vector and n is the unit normal vector to the natural boundary.

The constrained variational principle with penalty factors in axisymmetry conditions is as follows:

$$\begin{aligned} \Pi = 2\pi \left(\frac{1}{2} \int_{\Omega} (\mathbf{L}u)^T \cdot \mathbf{D}_e \cdot (\mathbf{L}u) \cdot r \, d\Omega - \int_{\Omega} u^T \cdot \mathbf{b} \cdot r \, d\Omega \right. \\ \left. - \int_{\Gamma_t} u^T \cdot \bar{\mathbf{t}} \cdot r \, d\Gamma \right) - \int_{\Gamma_u} \frac{1}{2} (\mathbf{u} - \bar{\mathbf{u}})^T \boldsymbol{\alpha} (\mathbf{u} - \bar{\mathbf{u}}) \, d\Gamma = 0 \end{aligned} \quad (18)$$

where $\boldsymbol{\alpha}$ is the identity matrix of penalty factors, Lu is the strain vector and D_e is the elastic property matrix of the material. For axisymmetry conditions:

$$\begin{aligned} \boldsymbol{\varepsilon}^T = (\mathbf{L}u)^T = [\varepsilon_r \quad \varepsilon_z \quad \gamma_{rz} \quad \varepsilon_\theta]^T \\ = \left[\frac{\partial u}{\partial r} \quad \frac{\partial w}{\partial z} \quad \frac{\partial u}{\partial z} + \frac{\partial w}{\partial r} \quad \frac{u}{r} \right]^T \end{aligned} \quad (19)$$

The stress vector can be easily obtained by:

$$\boldsymbol{\sigma}^T = \mathbf{D}_e (\mathbf{L}u) = [\sigma_r \quad \sigma_z \quad \tau_{rz} \quad \sigma_\theta]^T \quad (20)$$

Substituting (10) in (18) and performing some algebraic work, the discretized final form of system equations is derived as follows:

$$[\mathbf{K} + \mathbf{K}^\alpha] \mathbf{U} = \mathbf{F} + \mathbf{F}^\alpha \quad (21)$$

in which

$$K_{IJ} = 2\pi \int_{\Omega} B_I^T D_e B_J \cdot r \, d\Omega \quad (22)$$

$$B_I = \mathbf{L} \Phi_I = \begin{bmatrix} \phi_{I,x} & 0 & \phi_{I,y} & \phi_I / r \\ 0 & \phi_{I,y} & \phi_{I,x} & 0 \end{bmatrix} \quad (23)$$

$$\Phi_I = \begin{bmatrix} \phi_I & 0 \\ 0 & \phi_I \end{bmatrix} \quad (24)$$

$$\mathbf{f}_I = 2\pi \left(\int_{\Omega} \Phi_I^T \mathbf{b} \cdot r \, d\Omega + \int_{\Gamma_t} \Phi_I^T \bar{\mathbf{t}} \cdot r \, d\Gamma \right) \quad (25)$$

$$\mathbf{K}_U^\alpha = \int_{\Gamma_u} \Phi_I^T \boldsymbol{\alpha} \Phi_J \, d\Gamma \quad (26)$$

$$\mathbf{F}_I^\alpha = \int_{\Gamma_u} \Phi_I^T \boldsymbol{\alpha} \bar{\mathbf{u}} \, d\Gamma \quad (27)$$

In these equations, $\phi_{I,x}$, $\phi_{I,y}$ denote derivations of the

shape function with respect to x and y , accordingly.

III. NUMERICAL IMPLEMENTATION

The benchmark problem involves a hollow circular tube of inner radius a and outer radius b subjected to internal pressure p . The tube extends indefinitely along the z axis. The material is isotropic with elastic modulus E and Poisson's ratio ν . A slice of thickness h is extracted and noded as shown in Fig. 2.

The illustrated slice is vertically constrained at the top and bottom boundaries of the slice; thus each node can only move in the radial direction. In this study, the numerical procedure is carried out with the following input parameters: $a = 4$ m, $b = 10$ m, $h = 2$ m, $p = 10$ kPa, $E = 1000$ kPa with the nodal discretization shown in Fig. 2 and 1×4 equal integration elements each containing 5×5 Gauss points. The alpha constant in enforcing essential boundary condition (26) is opted as $1 \times 10^8 E$.

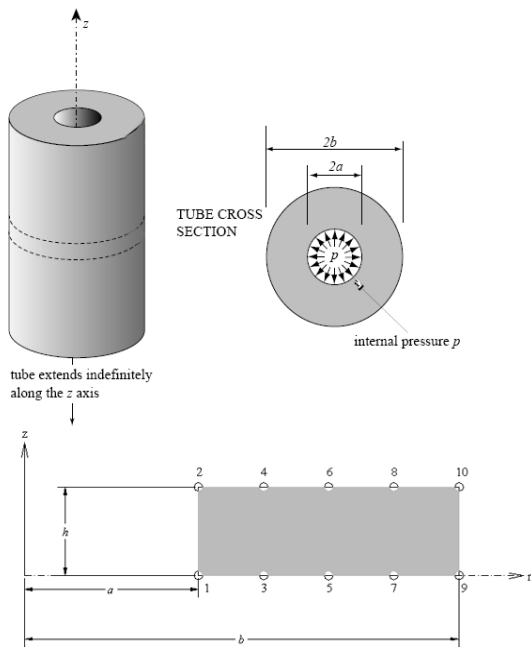
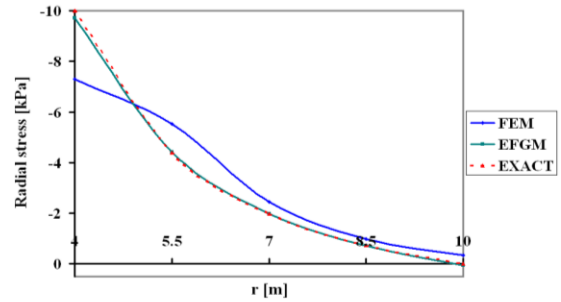


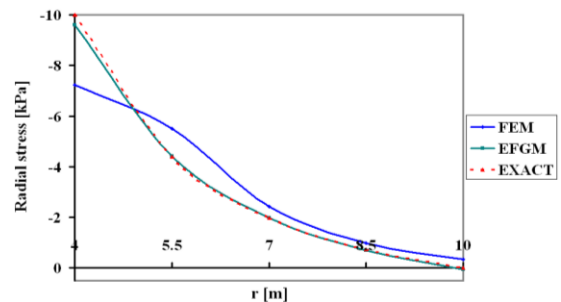
Fig. 2. Thick cylindrical tube under internal pressure

In order to check the validity of the results, they have been compared to closed form solutions obtained from [10]. For comparing the accuracy of the aforementioned EFG approach against another numerical method, the results are also compared to those of conventional FEM analysis with the same nodal positions as in Fig. 2 with 8 triangular CST elements. The results for radial stress and hoop stress for three Poisson's ratios are depicted in Figs. 3 and 4 respectively. The difference between the predicted radial displacements obtained from the two numerical methods and the closed-form solution is negligible and not discussed here; however, this is not the case for stresses. Figs. 3 and 4 show that the predicted hoop and radial stresses based on FEM diverge from closed-form solutions to some extent. It is also observed in Figs. 3 and 4 that for stresses, even in such sparse

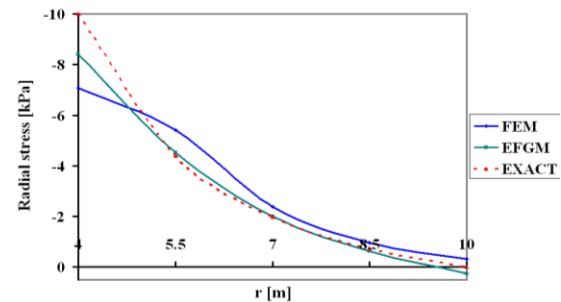
nodal positions, the predicted values of stresses based on EFG method satisfactorily fit the exact ones. Besides, as it is known, if Poisson's ratio is increased, for a given number of nodes, numerical results lose accuracy; however, it is shown in Figs. 3 and 4 that EFGM results act much better than FEM in high Poisson's ratios (i.e. $\nu = .45$) and show good consistency with analytical solution in these conditions. This is a prominent feature of this method compared to FEM.



(a)



(b)



(c)

Fig. 3. Radial stress (σ_r), (negative values denote compressive stresses); (a) $\nu=0$, (b) $\nu=0.2$, (c) $\nu=0.45$

This much higher accuracy of EFGM explained here seems interesting; however, a probable question that may arise is that under what conditions best results are obtained. To answer this question, one may take into account three sources of error: MLS shape functions, way of satisfying essential boundary conditions, and background mesh of integration. Research implemented by the authors show that the parameters involved with these sources are problem-based; which means there is not a unique rule to apply for all problems [11]. However, there are some guides which may become useful in acquiring more accurate results.

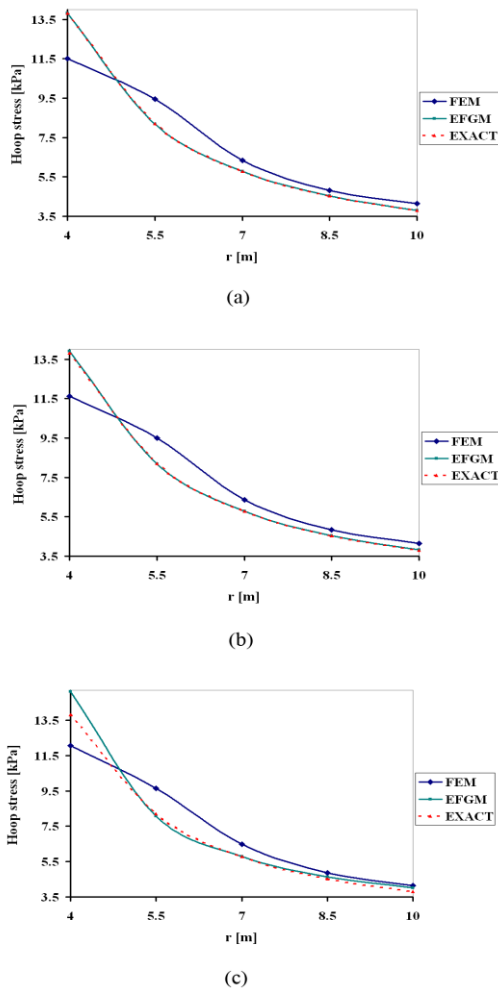


Fig. 4. Hoop stress (σ_θ); (a) $\nu=0$, (b) $\nu=0.2$, (c) $\nu=0.45$

To demonstrate the preceding allegations, two error indicators are defined here; one for displacements and the other for stresses.

$$\text{Disp norm} = \left\{ \int_{\Omega} (\mathbf{u}^{\text{NUM}} - \mathbf{u}^{\text{EXA}})^T (\mathbf{u}^{\text{NUM}} - \mathbf{u}^{\text{EXA}}) d\Omega \right\}^{\frac{1}{2}} \quad (28)$$

$$\text{Stress norm} = \left\{ \int_{\Omega} (\boldsymbol{\sigma}^{\text{NUM}} - \boldsymbol{\sigma}^{\text{EXA}})^T (\boldsymbol{\sigma}^{\text{NUM}} - \boldsymbol{\sigma}^{\text{EXA}}) d\Omega \right\}^{\frac{1}{2}} \quad (29)$$

where *NUM* and *EXA* superscripts stand for numerical and analytical values.

A. Effect of the Penalty Factor

In this problem, the introduced norms did not change by altering the penalty constant from $1 \times 10^3 E$ to $1 \times 10^8 E$. As this is usually the case for linear analysis [9], it has not been addressed herein.

B. Effect of the Size of Influence Domain

To study the MLS shape functions, the size of influence domain in (14) is varied by changing the influence factor, D_{\max} , identically for both directions from 1.5 to 1×10^9 . The node structure shown in Fig. 2 and 25 Gauss points per each cell of 1×4 background mesh are used in this study. The results are plotted in Figs. 5 and 6 for displacement and stress norms versus influence factor in a semi-logarithmic scale.

It is important to note that by increasing D_{\max} to infinity, the weight function of (9) becomes constant and its

derivatives get to zero.

Two apparent trends are seen in both of these Figures; an ascending trend from $D_{\max} = 1.5$ which leads to the least error (maximum accuracy) for $D_{\max} = 5.0$, and a descending trend from $D_{\max} = 5.0$ to infinity.

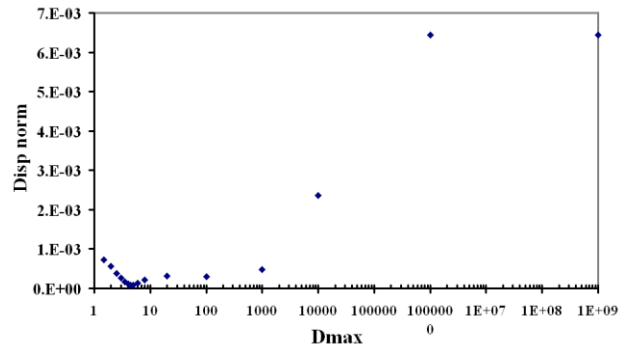


Fig. 5. Effect of the size of influence domain on displacement error

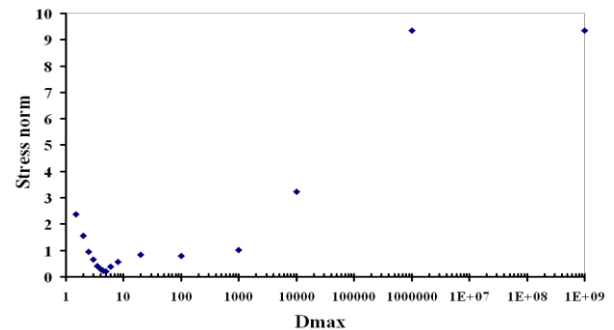


Fig. 6. Effect of the size of influence domain on stress error

There is not a unique agreement over the optimum value of the size of influence domain which gives most accurate results. In fact, this factor can vary in different problems.

The descending trend can be justified by taking a meticulous look at the MLS formulation in section II.A. By increasing the size of the influence domain, d_w , in (13) to infinity, the weight function in (12) becomes constant over the whole domain (as in standard Least Squares approximants); thus when differentiating the shape function of (9), the term $\mathbf{P}^T \mathbf{A}_{,x \text{ or } y}^{-1} \mathbf{B}_1 + \mathbf{P}^T \mathbf{A}^{-1} \mathbf{B}_{1,x \text{ or } y}$ limits to zero. This was the foundation of Diffuse Element Method by Nayroles et al [12]. Neglecting the above terms can cause a significant deviation from the accurate results; e.g. nearly %8000 and %4000 for displacements and stresses respectively in our benchmark problem.

C. Effect of Integration Points

Although the shape functions and their derivatives in (23) are not polynomials, it has been realized that by increasing the number of Gauss points, the integration accuracy generally improves. Yet, as stated before, this is not unconditionally true; because in [9] it is shown for elastic analysis of Timoshenko beam [10] that if the number of Gauss points exceeds some value, it can have some inverse effects on the accuracy. Further investigations done by the authors in elasto plastic analysis of an earth dam consent this [11]. However, in addition to the number of integration points, the arrangement of the background cells is also

decisive; in a way that in case of suitable arrangement of these cells, suitable results may be obtained with less number of Gauss points needed in each cell.

In order to have a better view over the integration points and their effect on the results, let us assume the regular set of 85 nodes illustrated in Fig. 7.

Now, let us consider 12 identical background cells for the integration mesh with the following arrangements: along z , along r : 1x12, 2x6, 3x4, 4x3. Thus, by varying the number of integration points in each cell, the ratio of total integration points to the total number of nodes, η (Eta), remains the same for all of these arrangements. Displacement & stress errors are plotted against this value for all of the mentioned arrangements in Figs. 8 and 9, accordingly.

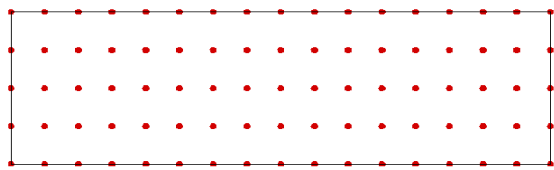


Fig. 7. Regular set of 85 nodes

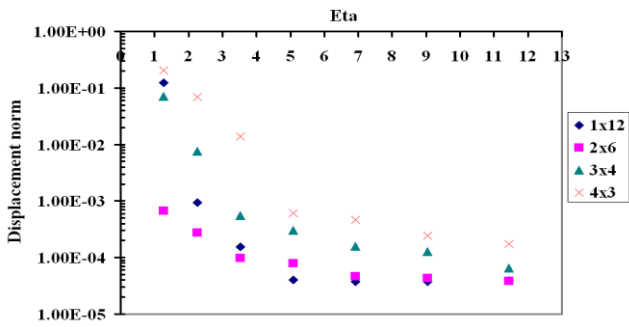


Fig. 8. Effect of cells arrangements and number of integration points on displacement error, 12 integration cells

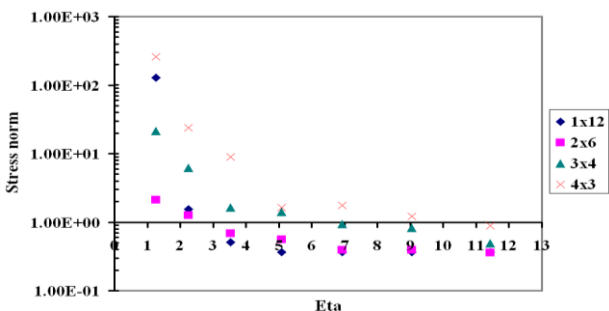


Fig. 9. Effect of cells arrangements and number of integration points on stress error, 12 integration cells

These Figures contain two hints; first is that by increasing the number of integration points, both errors decrease and the second is that by choosing a specific arrangement (2x6 here) for the background cells, the errors attenuate; e.g. the results obtained from 2x6 cells arrangement with 9 Gauss points per cell ($\eta=1.27$) are much more accurate than those obtained from 4x3 cells arrangement with 25 Gauss points per cell ($\eta=3.53$).

This explains that the accuracy of the method not only depends on the number of Gauss points and the Eta value, but also on the cells arrangement.

This finding is mostly disregarded in EFGM analyses. In other words, one can substantially reduce the computation time and increase the accuracy by proper arrangement of the

same number of integration cells. In this problem, which is isotropic and axisymmetric with infinite length along rotation axis, it seems that in order to get best results, the ratio of integration cells in longitudinal and transverse directions should be proportionate to the ratio of extension of the model geometry in the two directions. For instance, in the above benchmark problem, this ratio is $(b-a)/h=3$ and as seen from Figs. 8 and 9, least errors are obtained for 2x6 ($z:r$) cells arrangement. A further analysis with the same number and arrangement of nodes, i.e. 85 nodes, but with 48 background cells was done; which led to the results shown in Figs. 10 and 11. Again, most accuracy is obtained from 4x12 ($n_r/n_z=3$) cells arrangement.

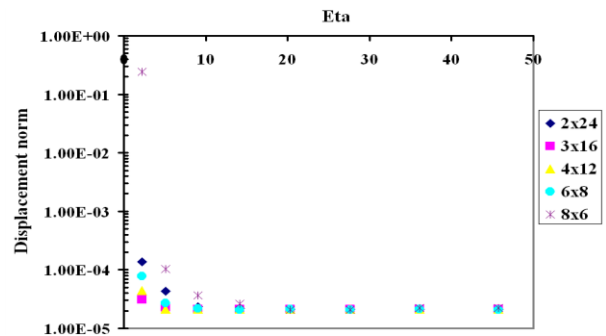


Fig. 10. Effect of cells arrangements and number of integration points on displacement error, 48 integration cells

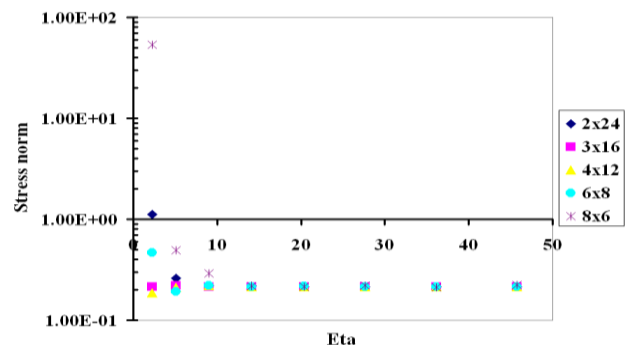


Fig. 11. Effect of cells arrangements and number of integration points on stress error, 48 integration cells

IV. SUMMARY

In this paper, EFGM formulation for analysis of axisymmetric problems was proposed and some aspects of this method were dealt with in an analysis of a benchmark problem. It was shown that, for the same number of nodes, EFGM provides significant accuracy in comparison with FEM. However, this accuracy depends mainly on proper choice of some parametric values. The effects of these values on the displacement and stress errors were investigated and it was found that there is an optimum value for the size of influence domain for which best results can be obtained. Deviation from this optimum value may result in loss of accuracy. Another point is that the integration precision in EFGM is not only dependent on the number of integration cells, but also on the arrangement of the background cells. The authors proposed that this arrangement should be commensurate to the geometry of the model for isotropic axisymmetric problems with infinite length along rotation axis.

REFERENCES

- [1] T. Belytschko, Y. Y. Lu, and L. Gu, "Element-Free Galerkin Methods," *International journal for numerical methods in engineering*, 1994, vol. 37, pp. 229-256
- [2] N. Sukumar, B. Moran, T. Black, and T. Belytschko, "An element-free Galerkin method for three-dimensional fracture mechanics," *Computational Mechanics*, 1997, vol. 20, pp. 170-175
- [3] I. V. Singh and B. K. Mishra and Mohit Pant, "A modified intrinsic enriched element free Galerkin method for multiple cracks simulation," *Materials & Design*, 2010, vol. 31, issue 1, pp. 628-632
- [4] S. Barry and S. Saigal, "A three-dimensional element-free Galerkin elastic and elastoplastic formulation," *Int. J. Numer. Meth. Eng.*, 1999, vol. 46, pp. 671-693
- [5] M. H. Kargarnovin, H. E. Toussi, and S. J. Fariborz, "Elasto-plastic element-free Galerkin method," *Computational Mechanics*, 2003, vol. 33, pp. 206-214
- [6] R. Rossi and M. Krajnc Alves, "On the Analysis of an EFG Method Under Large Deformations and Volumetric Locking," *Computational Mechanics*, 2007, vol. 39, no. 4, pp. 381-399.
- [7] S. A. Sadrnejad and A. N. Hayati, "Meshless analysis of an earth dam by Element-Free Galerkin method," in *Proc. International Conference on Scientific Computing (CSC'06)*, 2006, pp. 299-305
- [8] M. N. Oliaei and A. Pak, "Element free Galerkin meshless method for fully coupled analysis of consolidation process," *Scientia Iranica, Transaction A*, 2009,
- [9] G. R. Liu, "Mesh-free methods: moving beyond the finite element method," *CRC Press LLC*, 2002
- [10] S. P. Timoshenko and J. N. Goodier, "Theory of Elasticity, 3rd ed.," *McGraw-Hill*, 1970
- [11] A. N. Hayati, "Numerical analysis of an earth dam body by Element-Free Galerkin Method," *M.Sc. thesis, Faculty of Civil Engineering*, Khaje Nasir University of Technology, 2006
- [12] B. Nayroles, G. Touzot, and P. Villon, "Generalizing the finite element method: diffuse approximation and diffuse element," *Comput. Mech.*, 1992, vol. 10, pp. 307-318.